Conductance Modulation in Double Quantum Wells Due to Magnetic Field-Induced Anticrossing

J. A. Simmons, S. K. Lyo, N. E. Harff*, and J. F. Klem

Sandia National Laboratories, Albuquerque, New Mexico 87185

We observe a strong modulation of the low temperature in-plane conductance $G_\parallel$ of coupled quantum wells (QW's) by an in-plane magnetic field $B_\parallel$ and attribute this to an anticrossing of the two QW dispersion curves. The anticrossing produces a partial energy gap, yielding large, $B_\parallel$-tunable distortions in the Fermi surface and density of states. Sweeping $B_\parallel$ moves the energy gap through the Fermi level, with the upper and lower gap edges producing a sharp maximum and minimum in $G_\parallel$, in agreement with theoretical calculations. The gap energy is directly determined from the data.

The unique experimental properties of double quantum well (DQW) structures arise from the fact that the two parallel two-dimensional electron gas (2DEG) layers contain an additional electronic degree of freedom in the growth direction. Thus an electron occupies either the top or bottom quantum well (QW), or in the case of balanced QW densities the symmetric or antisymmetric state. This additional degree of freedom can be controlled by varying the thickness of the barrier between the two QW's, as well as by applying external gate voltages and magnetic fields. DQW's thus provide an ideal platform for studying the tunneling dynamics between two parallel 2DEG's.

In high magnetic fields perpendicular to the growth plane $B_\perp$, the electrons' kinetic energies are quenched and Coulomb interactions dominate, leading to a tunneling gap [1] in the interwell tunneling conductance $G_\perp(B_\perp)$ and observation of a Coulomb-driven correlated bilayer state [2,3] in the in-plane conductance $G_\parallel(B_\perp)$. By contrast, in a purely in-plane field $B_\parallel$, single particle tunneling dynamics dominate the interactions between the two 2DEG's. The primary effect of $B_\parallel$ is a linear transverse shift in the canonical momentum $\hbar k$ of electrons in one QW relative to the other. This produces a strong modulation [4–7] of the tunneling conductance $G_\perp(B_\parallel)$ due to the conservation of energy and k. To date, however, the *in-plane* conductance $G_\parallel$ of coupled DQW's in $B_\parallel$ has received little attention [8].

Here we report clear observation of a partial energy gap (PEG) in strongly coupled DQW's due to a $B_\parallel$-induced anticrossing of the two QW's dispersion curves [9]. $B_\parallel$ causes a linear transverse shift in k of the dispersion curve of one QW relative to the other, resulting in an anticrossing and the opening of a PEG when the coupling is sufficiently strong. Under these conditions the DQW has a multicomponent Fermi surface whose shape and topology are tunable by $B_\parallel$. The electronic density of states $D(\varepsilon)$ and group velocities are dramatically distorted at the upper and lower edges of the PEG (e.g., a Van Hove singularity appears). Sweeping $B_\parallel$ causes the gap to pass through the chemical potential μ,

resulting in two large sharp features in $G_\parallel$, a maximum and minimum, corresponding to the upper and lower gap edges, respectively [10]. The $B_\parallel$'s at which the features appear depend on surface gate bias in good agreement with a simple model and allow the gap energy ε_G to be directly determined. Theoretical calculations of $G_\parallel$ are consistent with the data. In addition, $G_\parallel$ is found to depend strongly on the angle between the applied electric field and $B_\parallel$, due to the highly anisotropic Fermi surface. We note that this Fermi surface is similar to that observed in tilted Si inversion layers nearly two decades ago [11], except that the present Fermi surface is tunable with $B_\parallel$.

We studied three modulation-doped DQW structures (A, B, and C), each consisting of two GaAs QW's of equal width w separated by an $Al_{0.3}Ga_{0.7}As$ barrier of thickness t. Table I lists the values of w and t, and the densities n_1, n_2 and mobilities μ_1, μ_2 of the top and bottom QW's, respectively, for gate voltages $V_G = 0$. Four terminal low-frequency lock-in measurements were performed at $T = 0.3$ K on Hall bars with Cr/Au top gates. n_1 and n_2 were determined from the quantum Hall effect and Shubnikov–de Haas (SdH) oscillations in $B_\perp$, followed by a rotation *in situ* for measurement in $B_\parallel$, with the residual component of $B_\perp$ less than 0.005 T.

The central experimental result of this paper is shown in Fig. 1. The inset depicts the in-plane resistance at $B_\parallel = 0$ of a 12 □ section of sample A as a function of V_G. A weak plateau appears at $V_G = V_{depl} \approx -0.29$ V, when only the top QW is depleted. Similarly, in $B_\perp$ the beatings in SdH oscillations characteristic of two 2DEG layers [8] disappear for $V_G \leq -0.29$ V. Figure 1 shows

TABLE I. Sample parameters.

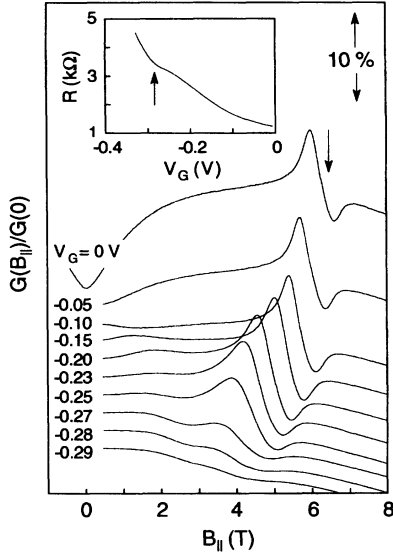| Sample	w/t (Å)	n (10^{11} cm^{-2}) n_1	n_2	μ (10^5 cm^2/V s) μ_1	μ_2
A	150/25	1.4	1.5	2.7	2.2
B	100/35	1.2	1.2	1.2	0.6
C	150/15	0.7	0.9	0.6	0.2

FIG. 1. Normalized $G_\parallel$ vs $B_\parallel$ of sample A for different V_G, offset from one another by 2%. Arrow indicates $\hbar c(k_1 + k_2)/ed$ for $V_G = 0$, with d from a Hartree self-consistent calculation. Inset: zero-field resistance vs V_G. Arrow indicates V_{depl}.

the normalized $G_\parallel(B_\parallel)$ for several different negative V_G. For $V_G = 0$, a sharp maximum appears at $B_{\mathrm{max}} \approx 5.8$ T, followed by a sharp minimum at $B_{\mathrm{min}} \approx 6.4$ T. As V_G decreases, both features move to lower $B_\parallel$, with B_{max} moving more rapidly than B_{min}. The strength of the features decreases once $V_G \lesssim -0.2$ V, until at $V_G \approx V_{\mathrm{depl}}$ they almost completely disappear. For all samples, once the top QW is depleted $G_\parallel$ is only weakly monotonic in $B_\parallel < 14$ T. This rules out as a source of the features the formation of cyclotron orbits within the individual QW's, expected semiclassically when $B_\parallel > 4\hbar c/ew^2$ (≈ 12 T for sample A). Thus the features are due solely to inter-QW interactions.

The data can be understood by noting that $B_\parallel$ (in the x direction) displaces the transverse crystal momenta k_y of one QW relative to that of the other by $\Delta k_y = edB_\parallel/\hbar c$, where d is the center-to-center distance between the two 2DEG layers. This results in an anticrossing of the two dispersion curves due to tunneling between the QW's, as shown in Fig. 2. We now calculate the effect of the anticrossing on $D(\varepsilon)$. The Hamiltonian is given by the sum of $\varepsilon_x(k_x) = \hbar^2 k_x^2/2m^*$ and

$$H = \frac{p_z^2}{2m^*} + \frac{\hbar^2}{2m^*}\left(k_y - \frac{eBz}{\hbar c}\right)^2 + V(z), \qquad (1)$$

where the effective mass m^* is assumed equal in the QW's and barrier, and $V(z)$ is the square-well DQW potential. The effect of a Hartree potential will be discussed later. For narrow QW's, only the two lowest eigenvalues $\varepsilon_\pm(k_y)$ of Eq. (1) are relevant. For a sym-

metric DQW structure $\varepsilon_\pm$ corresponds to the symmetric (ε_-) and antisymmetric (ε_+) ground states. The eigenvalues $\varepsilon_\pm(k_y)$ in the tight-binding approximation for $w = 150$, Å $t = 25$ Å, and unequal QW depths of 280 and 278 meV, corresponding roughly to sample A with $V_G \approx -0.1$ V, are shown on the left of Fig. 2 for $B_\parallel = 0$, 0.7, and 7.5 T. At $B_\parallel = 0$ the $\varepsilon_\pm(k_y)$ curves are parabolic and $D(\varepsilon)$ is constant for each energy branch, with the energy splitting between the two branches due to both the unequal QW depths and tunneling (i.e., mixing or coupling) [see Fig. 2(a)]. For $B_\parallel = 0.7$ and 7.5 T, in the absence of coupling the Fermi circles tough tangentially on the inside and outside, respectively, at the same $\mu \approx 6.3$ meV, corresponding to $\Delta k_y = k_1 \pm k_2$. These two cases exhibit two types of anticrossings: Type I occurs when $\Delta k_y < \max(k_1, k_2)$, shown in Fig. 2(b). Near the anticrossing, the slopes of $\varepsilon_\pm(k_y)$ deviate but do not change sign, only slightly changing the group velocity. Further, the changes in $D(\varepsilon)$ due to each energy branch cancel one another. Thus the effect on $G_\parallel(B_\parallel)$ of a type I anticrossing passing through μ is negligible, in accord with the data of Fig. 1, for which no features appear at $B_\parallel = \hbar c(k_1 - k_2)/ed$.

A type II anticrossing occurs when $\Delta k > \max(k_1, k_2)$, as shown in Fig. 2(c). In this case the slopes of $\varepsilon_\pm(k_y)$ change sign, and a PEG of width $\varepsilon_G \approx 2$ meV appears. For high fields ε_G is insensitive to $B_\parallel$ and is due mainly to mixing. Hence $\varepsilon_G \approx \Delta_{\mathrm{SAS}}$, the $B_\parallel = 0$ symmetric-antisymmetric gap observed when the QW depths (densities) are equal [2]. (As discussed later, ε_G and Δ_{SAS} decrease to ~ 1.4 meV when the Hartree potential is in-
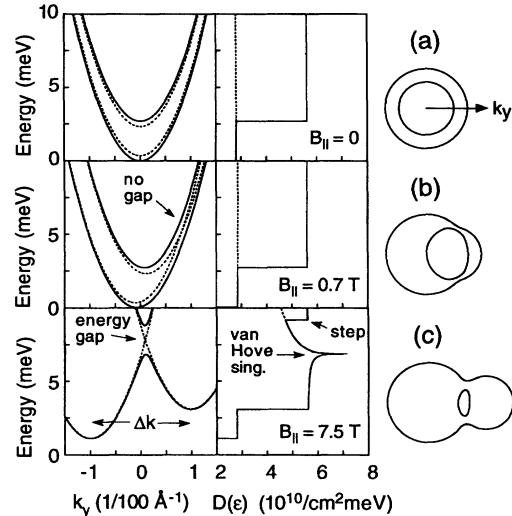

FIG. 2. For sample A, calculated dispersion $\varepsilon(k_y)$ (left) both with (solid lines) and without (dotted lines) mixing; calculated density of states $D(\varepsilon)$ (middle) for lower energy branch (dotted line) and both energy branches (solid line); and sketch of Fermi surface for $\mu \approx 8$ meV (right); for $B_\parallel = $ (a) 0 T, (b) 0.7 T, and (c) 7.5 T.

cluded.) The gap produces dramatic distortions in the electron group velocities and $D(\varepsilon)$. At the upper gap edge the dispersion is nearly parabolic and a sharp steplike reduction appears in $D(\varepsilon)$. States at the upper gap edge have low velocities and contribute little current, yet make significant contributions to the scattering rates of electrons elsewhere on the Fermi surface. As $B_{\parallel}$ increases, pushing the upper gap edge through μ, electrons are no longer scattered into these states, yielding the observed maximum in $G_{\parallel}$. The lower gap edge, by contrast, has a saddle-shaped dispersion of the form $\varepsilon(k_x, k_y) = \varepsilon_0 + (\hbar k_x)^2/2m^* - (\hbar k_y)^2/2m'$, where ε_0 is the saddle-point energy, and m' is determined by the saddle-point curvature. This form produces a Van Hove singularity at ε_0, resulting in $D(\varepsilon)$ becoming infinite as $D(\varepsilon) \propto \ln|\varepsilon - \varepsilon_0|$, as shown in Fig. 2(c). Since the saddle-point states have zero group velocity, when $B_{\parallel}$ is swept and the lower gap edge passes through μ, electrons are divergently scattered into states that carry no current, yielding the sharp minimum in $G_{\parallel}$.

Following this qualitative discussion, we calculate $G_{\parallel}(B_{\parallel})$, in the direction $\mathbf{u}$ of an applied external electric field, using [10]

$$G_{\parallel} = \frac{2e^2}{A} \sum_{\mathbf{k}} (\mathbf{u} \cdot \mathbf{v_k})^2 [-f_{\mathbf{k}}'] \tau_{\mathbf{k}} . \qquad (2a)$$

Here $\tau_{\mathbf{k}}$ is the relaxation time given by

$$\tau_{\mathbf{k}}^{-1} = \frac{2\pi N_I}{\hbar} \sum_{\mathbf{k}} \langle |V_{\mathbf{k'k}}|^2 \rangle \delta(\varepsilon_{\mathbf{k}} - \varepsilon_{\mathbf{k'}}), \qquad (2b)$$

where $\mathbf{v_k} = \hbar^{-1} \nabla_{\mathbf{k}} \varepsilon_{\mathbf{k}}$, $\varepsilon_{\mathbf{k}} = \varepsilon_x(k_x) + \varepsilon_{\pm}(k_y)$, $\mathbf{k}$ includes implicitly the indices $\pm$ for the upper and lower energy branches, and A is the area of cross section of the QW's. Here N_I is the total number of randomly distributed static scattering centers, and $f_{\mathbf{k}}' = f'(\varepsilon_{\mathbf{k}})$ is the energy derivative of the Fermi function. The matrix element $V_{\mathbf{k'k}}(z)$ of the impurity scattering is assumed to be isotropic. The angular brackets in Eq. (2b) denote the average over the impurity distribution. Though the scattering-in term should be included in a more general situation, our purpose here is to demonstrate qualitatively the features in the data. Accordingly we make a further simplifying approximation by ignoring the momentum dependence of $V_{\mathbf{k'k}} = V_I$, obtaining $\tau^{-1}(\varepsilon) = \pi V_I^2 N_I D(\varepsilon)$, where $D(\varepsilon)$ includes spin.

Figure 3 shows an evaluation of Eq. (2) for $w = 150$ Å, $t = 25$ Å, and $n_1 = n_2 = 1.5 \times 10^{11}$ cm^{-2}, corresponding to sample A at $V_G \approx 0$. $G_{\parallel}$ exhibits the sharp maximum and minimum corresponding to the upper and lower PEG edges passing through μ. Three different ratios of the scattering times in the upper (τ_u) to lower (τ_l) energy branches are shown. A numerical calculation, based on Eq. (2b), of $G_{\parallel}$ in the presence of two delta-impurity sheets at the left interfaces of the QW's shows only negligible de-
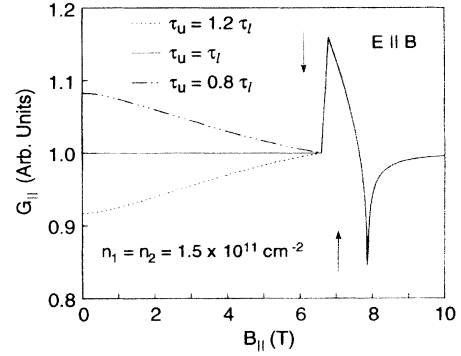

FIG. 3. Calculated $G_{\parallel}$ vs $B_{\parallel}$ for a symmetric DQW with $w = 150$ Å, $t = 25$ Å, and conduction band offsets of 280 meV, similar to sample A at $V_G \approx 0$. Here τ_u and τ_l are the scattering times in the upper and lower branches. The maximum and minimum move to the positions indicated by arrows when the Hartree potential is included.

viations from the $\tau_u = \tau_l$ approximate result. The features are rounded when damping is included. In a Hartree self-consistent calculation (HSCC), the effective d is increased from 175 to 195 Å, and $B_{\max}$ and $B_{\min}$ are reduced by this ratio to the positions indicated by the arrows, yielding good qualitative agreement with the data.

We now turn to the effects of gate bias. In Fig. 4 we plot $B_{\mathrm{mid}} = (B_{\min} + B_{\max})/2$ vs V_G for all three samples. B_{mid} corresponds roughly to the field $\hbar c(k_1 + k_2)/ed$ at which μ lies in the middle of the PEG. To a first approximation, negatively biasing V_G linearly decreases n_1 while leaving n_2 unchanged. This simple model gives
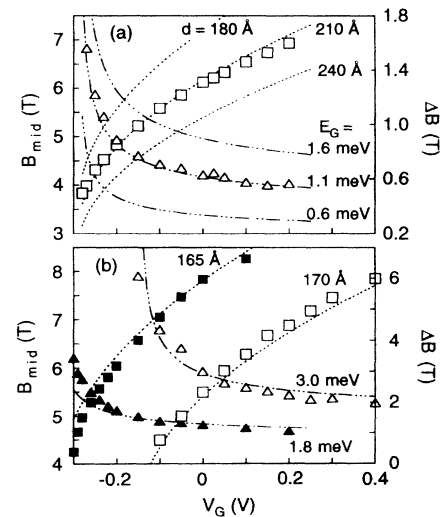

FIG. 4. (a) Plot of B_{mid} (squares) and ΔB (triangles) for sample A. Using sample A parameters, dotted lines are plots of Eq. (3) for various d, while dash-dotted lines are plots of Eq. (4) for various ε_G. (b) Same as in (a), but for samples B (solid symbols) and C (open symbols), and only showing the best fits.

B_{mid} as

$$B_{\text{mid}} = \left(\sqrt{\frac{C_G}{e} (V_G - V_{\text{depl}})} + \sqrt{n_2} \right) \frac{\hbar c \sqrt{2\pi}}{ed}, \quad (3)$$

where C_G is the real capacitance between the gate and top QW calculated from the samples' growth structures, and n_2 and V_{depl} are known from gate scans and measurements in $B_\perp$. In Fig. 4 we show fits of Eq. (3) to the B_{mid} data, with d as the only adjustable parameter. HSCC's give values for d of 195, 140, and 180 Å for samples A, B, and C, respectively, in relatively good agreement with the data.

Also plotted in Fig. 4 are $\Delta B = B_{\text{min}} - B_{\text{max}}$ for the three samples. Using the same model and assuming that B_{max} and B_{min} occur at $\hbar c [k_1 + k_2 \pm (\Delta k_1 + \Delta k_2)]/ed$, where $\Delta k_{1,2} = \varepsilon_G/(2 \partial \varepsilon / \partial k_{1,2})$ and $\partial \varepsilon / \partial k_{1,2}$ is evaluated as $(2\pi n_{1,2})^{1/2} \hbar^2 / m^*$, we obtain

$$\Delta B = \left[\left(\frac{C_G}{e} (V_G - V_{\text{depl}}) \right)^{-1/2} + n_2^{-1/2} \right] \frac{E_G m^* c}{ed\hbar \sqrt{2\pi}}. \quad (4)$$

Fits of Eq. (4) to the ΔB data, using the values for d obtained from the fit of Eq. (3) to B_{mid}, are shown as dash-dotted lines, with ε_G as the only adjustable parameter. The best fits for samples A, B, and C are obtained for $\varepsilon_G = 1.1$, 1.8, and 3.0 meV. These are in fair agreement with the values of 1.4, 2.0, and 3.4 meV obtained from the HSCC's, demonstrating that ε_G can be directly obtained from the data. Since the approximations used in Eq. (4) break down as ε_G becomes large, the discrepancy is largest for sample C.

The data shown until now have all been for an angle $\theta = 0°$ between the direction u of applied electric field and $B_\parallel$. Because the Fermi surface is highly anisotropic, and also because of the $(\mathbf{u} \cdot \mathbf{v_k})^2$ factor in Eq. (2a), we expect a large anisotropy in $G_\parallel$ with θ. In Fig. 5 we show $G_\parallel$ of sample B for several values of θ. (Because θ was varied by etching multiple Hall bars on the same chip, $B_\perp$ was kept below 0.005 T and equal for all θ.) As expected, $G_\parallel$ shows an unusually large degree of anisotropy, with the size of the anticrossing features for $\theta = 90°$ approaching 30%, nearly a factor of 3 larger than for $\theta = 0°$.

In summary, we have observed an anticrossing of the two QW dispersion curves in strongly coupled DQW's in $B_\parallel$. The resulting energy gap produces a sharp decrease in $D(\varepsilon)$ at the upper gap edge, and a singularity in $D(\varepsilon)$ at the lower gap edge. Sweeping $B_\parallel$ moves the gap through the Fermi level, with the upper and lower gap edges producing a sharp maximum and minimum in $G_\parallel$, in agreement with theoretical calculations. The gap energy
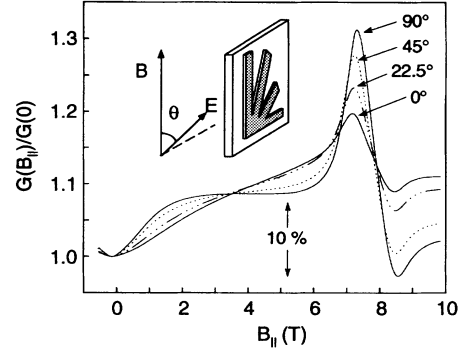

FIG. 5. Normalized $G_\parallel(B_\parallel)$ of sample B, for several different angles θ between the direction u of electric field and $B_\parallel$. Inset: experimental geometry.

can be directly determined from the V_G dependence of the features in $G_\parallel$. This greatly distorted dispersion should produce large deviations in the electron effective masses near the energy gap, making this an interesting area for future study.

*Also at Oregon State University, Corvallis, OR 97331.
[1] J. P. Eisenstein, L. N. Pfeiffer, and K. W. West, Phys. Rev. Lett. **68**, 3804 (1992).
[2] G. S. Boebinger et al., Phys. Rev. Lett. **64**, 1793 (1990); Y. W. Suen et al., Phys. Rev. B **44**, 5947 (1991).
[3] A. H. MacDonald, P. M. Platzman, and G. S. Boebinger, Phys. Rev. Lett. **65**, 775 (1990); L. Brey, Phys. Rev. Lett. **65**, 903 (1990).
[4] J. P. Eisenstein et al., Phys. Rev. B **44**, 6511 (1991).
[5] J. A. Simmons et al., Phys. Rev. B **47**, 15 741 (1993); S. K. Lyo and J. A. Simmons, J. Phys. Condens. Matter **5**, L299 (1993).
[6] J. Smoliner et al., Phys. Rev. Lett. **63**, 2116 (1989).
[7] K. M. Brown et al., Appl. Phys. Lett. **64**, 1827 (1994).
[8] G. S. Boebinger et al., Phys. Rev. B **43**, 12 673 (1991), studied Fermi-surface distortions through $B_\parallel$-induced changes in Shubnikov–de Haas oscillations in $B_\perp$, but $B_\parallel$ was too small to produce an anticrossing energy gap.
[9] M. Helm et al., Phys. Rev. B **39**, 3427 (1989), observed weak anticrossings in double barrier resonant tunneling structures in $B_\parallel$, but did not see an energy gap.
[10] S. K. Lyo, Phys. Rev. B **50**, 4965 (1994).
[11] T. Cole, A. A. Lakhani, and P. J. Stiles, Phys. Rev. Lett. **38**, 722 (1977); T. G. Matheson and R. J. Higgins, Phys. Rev. B **25**, 2633 (1982), and references therein.
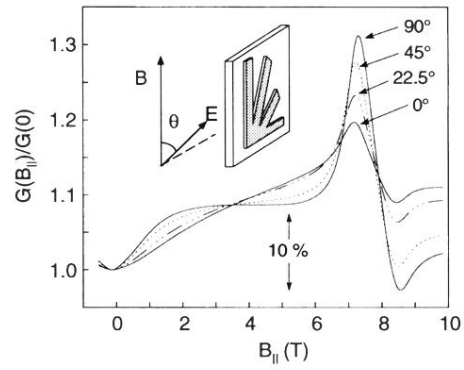
FIG. 5. Normalized $G_{\parallel}(B_{\parallel})$ of sample B, for several different angles θ between the direction $\mathbf{u}$ of electric field and $B_{\parallel}$. Inset: experimental geometry.